Optics & Laser Technology 176 (2024) 111018

Contents lists available at ScienceDirect

Optics and Laser Technology

journal homepage: www.elsevier.com/locate/optlastec

Full length article

Silicon rib waveguide with palladium coated gold nanorods overlayer for hexane and N-methylaniline detection

Anastasia Novikova, Aviad Katiyi, Alina Karabchevsky *

School of Electrical and Computer Engineering, Ben-Gurion University of the Negev, Beer-Sheva, 8410501, Israel

ARTICLE INFO

Keywords:
Palladium nanorods
Vibrational spectroscopy
Rib waveguide
Sensing
N-methylaniline
Hexane

ABSTRACT

The adsorption of hexane and N-methylaniline was investigated by on-chip vibrational spectroscopy. The interaction with the Pd surface significantly perturbs the vibrational modes of hexane. Near-infrared absorption spectroscopy on the waveguide detected a redshifted C–H stretching vibration. We showed that while rapid evaporation of one component may occur, the modification facilitates the sensing for large molecules and mixtures of substances. Rib waveguides were modified with palladium to exhibit an enhanced electromagnetic field effect due to the electrostatic interaction of Pd and hydrogen, showing the drop in the amine overtone absorption of 7.6 dB and the overtone related to the bond of carbon to hydrogen of 6.8 dB. The absorption of hexane bonds in water is 5.5 dB. The obtained values are 100 times higher than those predicted by the electromagnetic simulator for pure rib waveguides. This may be explained by C–H bonds in hexane that can be activated through a hydrogen bond-like interaction with metal substrates. This achievement holds promising potential for advancing hexane and N-Methylailine detection and analysis technologies, with implications for diverse applications in various industries, such as environmental monitoring, industrial processes, and safety measures.

1. Introduction

Absorption spectroscopy-based trace sensing technology has found widespread application across various domains, including drug efficiency monitoring, industrial manufacturing, flow field analysis and others. Its utilization is attributed to its ability to leverage molecular "fingerprint" features, providing high selectivity, rapid response times, and enabling in-situ real-time detection [1]. The examination of alkane molecule adsorption on transition-metal surfaces has received considerable attention. For instance, the activation of C–H bonds within cyclohexane can occur via a hydrogen bond-like interaction with metal substrates (C–H···M interaction), leading to a significant redshift in the C–H stretching modes of adsorbed alkanes. Consequently, vibrational spectroscopy methods have primarily explored the relationship between alkanes and transition-metal surfaces.

Over the recent years, the international community has grappled with the urgent issue of the diminishing quality of our air, soil, and water resources [2,3]. With the increase in consumption of various raw materials and the development of technology, technologies for determining substances in various environments are being developed in parallel. With increasing rates of raw material processing and accelerating production cycles, the need arises for reliable methods for detecting volatile substances that either evaporate or quickly transform into more toxic compounds. Spectroscopic methods allow for determining substances at the speed of light [4,5] depending on the production tasks, various selective, sensitive, and long-lasting sensors are designed for liquid [6–10], gaseous [11], or solid states detection and for different application such as chemical, microbiological, food, fuel, petrochemical, pharmaceutical, pulp and paper, space, engineering, and metalworking industries; electric power, agriculture, and other detections. Planar waveguides stand out as promising research avenues with excellent prospects. Their unique design and characteristics make them intriguing subjects for further exploration and development within various scientific and technological applications [12–14].

N-methylaniline is a pollutant that can adversely affect the aquatic environment, soil, and air [15]. This chemical, belonging to the family of aromatic amines, has the potential to contaminate water bodies, leading to aquatic pollution. When released into the soil, it can contribute to soil pollution, impacting the health of plants and other organisms in the ecosystem. Moreover, in vapor form, methyl aniline can be released into the air, adding to air pollution concerns. N-methylaniline, a derivative of aniline, serves a dual role as both a latent and binding solvent and plays a crucial intermediate role in producing dyes, agrochemicals, and various other organic compounds. It can

* Corresponding author.
E-mail address: alinak@bgu.ac.il (A. Karabchevsky).

https://doi.org/10.1016/j.optlastec.2024.111018
Received 15 February 2024; Received in revised form 31 March 2024; Accepted 10 April 2024

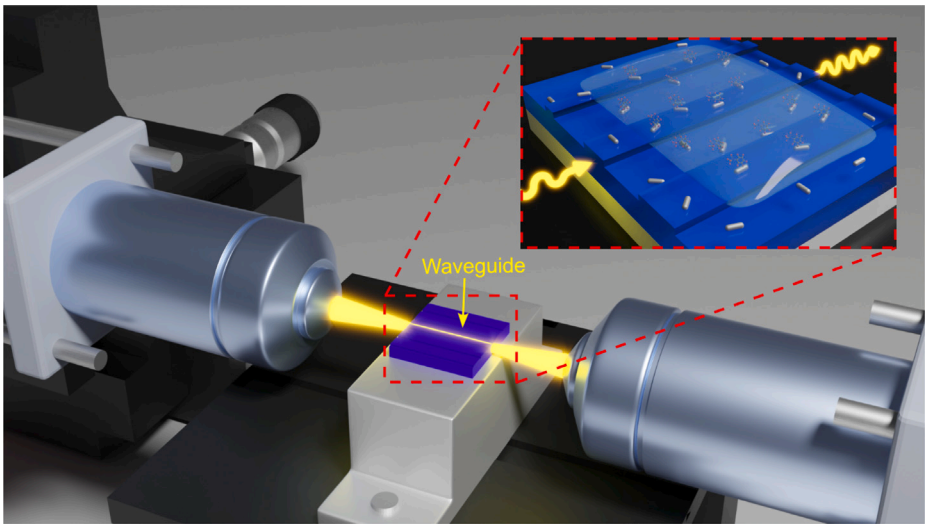

Fig. 1. Illustration of the experimental setup. The inset shows a magnified image of a rib waveguide with Pd + Au nanorods and a droplet of N-methylaniline.

enter the environment with wastewater from the dyeing industry and organic synthesis. However, it is essential to note that N-methylaniline is a highly toxic substance, classified as a fire hazard and considered hazardous. Exposure to this chemical can damage the central nervous system and has a potential risk of liver and kidney failure [16,17].

Hexane is an organic substance. It is a saturated hydrocarbon belonging to the class of alkanes, otherwise paraffin, aliphatic hydrocarbons [18]. Indeed, hexane shares characteristics with N-methylaniline in terms of its potential hazards. Hexane is known to be explosive and highly volatile, a fire hazard, and quickly evaporates into the air. It finds application in the synthesis of gasoline and other industrial processes. However, it is essential to note that hexane, like many volatile organic compounds, poses environmental risks and can contribute to pollution. When exposed to the body, it affects the central and peripheral nervous systems and the respiratory system [19,20].

Optical waveguides can be used for sensing those materials. Here, we show how the rib waveguide architecture modified with Pd nanorods allows for sensing on a chip. A rib waveguide is made of a guiding layer composed of a slab with one or more strips on the top [21–24]. Likewise, rib waveguides offer two-dimensional wave confinement, and in multi-layer strip structures, near-complete confinement can be achieved [25,26]. They are widely used in various applications, including telecommunications [27] and integrated optics [28]. Moreover, a rib waveguide can incorporate strips of varying heights and widths on one surface and can be divided into different sections. This feature enhances its selectivity in detecting various substances since different waveguide sections can be tailored to distinct substances. Furthermore, besides their inherent selectivity, rib waveguides can boost their sensitivity through surface modifications. When modified with various nanoparticles, a rib waveguide demonstrates promising potential for sensing applications, for example, for biochemistry, ecology, and chemistry [22,29–33]. Various metals can be used to modify rib waveguides and increase their sensitivity, namely gold, silver, aluminum, and rarely palladium. In addition to nanoparticles, films of metals (gold [34], silver [35], palladium [36], titanium dioxide [37]) and carbon-containing materials (graphene [38,39], MXene [40], polymers [41,42]) are used to modify the surfaces of waveguides. However, they provide one layer when nanoparticles can provide a more complex and larger specific surface area.

Aluminum [43] and silver [44] nanoparticles can be used to modify waveguide surfaces but are less stable in liquid and gaseous media and are easily oxidized. However, aluminum oxide nanoparticles are stable and can be used with other materials to modify the surfaces of waveguides. Gold [45] and palladium nanoparticles perform well for various sensing applications since they do not oxidize and have good chemical stability. Also, in the case of palladium, a considerable advantage is that it very quickly adsorbs hydrogen and all substances with hydrogen bonds onto its surface [46]. Increasing the sensor's specific surface area with palladium will increase its sensitivity, including mixtures containing rapidly evaporating substances. Also, a good solution for increasing sensitivity and reducing the cost of the material can be a combination of metals, in our case, nanorods composed of palladium and gold. More complex structures, such as nanorods, may also contribute to the detection of the substances under study due to their surface area.

Here, we report the design, fabrication, and demonstration of rib waveguides modified by gold (Au) nanorods coated with a layer of palladium (Pd), as illustrated in Fig. 1. The diameter of the Pd+Au nanorods is 25 nm and the length is 75 nm with a concentration of 100 μg/ml on the surface. The concept of employing palladium for surface modification of waveguides stemmed from its favorable interaction with hydrogen, which increases the adsorption of more molecules containing hydrogen bonds onto the waveguide surface, along with its efficient release of hydrogen during thermal or physical treatments. This increases the service life, sensitivity, selectivity to substances containing hydrogen bonds, and the service life of the waveguide. These reliable waveguides offer the capability for real-time operation and convenient detection of chemical, medical, and biological entities. In our research, we employed the concept of a modified rib waveguide to identify the absorption of N-methylaniline ($C_6H_5NH(CH_3)$) and Methylaminobenzene [47] within a hexane (C_6H_{14}) mixture of different concentrations.

2. Materials and methods

In the following section, we describe the materials and methods used in this study.

2.1. Materials

N-methylaniline ($C_6H_5NH(CH_3)$, ≥98%), Gold (Au) nanorods palladium (Pd) coated (25 nm diameter and 75 nm length with concentration of 100 μg/ml in water) and Hexane (C_6H_{14}, ≥95%) were purchased from Sigma-Aldrich, distilled water.

2.2. Fabrication of the chip-scale sensing device

The waveguide was fabricated on a silicon wafer with a silica thickness of 2 μm and silicon thickness of 2 μm. A hard mask of aluminum with a thickness of 50 nm was fabricated on the top of the wafer to create different-width strips with a height of 400 nm. Next, the wafer was dry-etched with SF_6+Ar and O^2. The residue of the hard mask was removed using a 400K developer. In the last step, the waveguide was covered with Tantalum pentoxide (Ta_2O_5) film with a thickness of 10 nm to protect the silicon waveguide. The rib waveguide was modified by gold nanorods palladium coated deposited on top of it. First, We cleaned the surface of the waveguide by placing it in acetone for 15 min and drying it at a temperature of 25C in a closed Petri dish. Next, the nanorods were dipped into the clean waveguide, which was dried in a closed petri dish.

2.3. Preparation of the analyte samples

N-methylaniline was mixed with hexane in 5 ml glass flasks in a few ratios of N-methylaniline to hexane; 1:1, 1:3, 1:5, and 1:10 while each part was equivalent to 200 ml. The solutions were stored at room temperature (25C) in a laminar flow hood.

2.4. Experiment optical set-up

A broadband laser source (NKT SuperK EXTREME), a wavelength range from 400 nm to 2400 nm, was coupled to a single-mode fiber through an Olympus plan achromat objective featuring a numerical aperture (NA) of 0.25 and a magnification of x10. The fiber was then attached to a silver reflective collimator with a beam diameter of 2 mm, producing a collimated beam. This setup provides a means to efficiently couple the laser light into the single-mode fiber for various optical applications within the specified wavelength range. The collimated beam generated was directed onto the input face of the rib waveguide employing a microscope objective characterized by a long working distance, magnification of x100, numerical aperture of 0.55, and a working distance of 13 mm. The input coupling arrangement was integrated with the rib waveguide through a 3-axis NanoMax Stage. The customized rib waveguide, positioned on a 3-axis stage (MicroBlock MBT616D), featured a 2-axis rotary stage for precise angular alignment. An experimental apparatus was constructed to ensure the alignment of optical components. The output beam was collected using the same objective as the input one. The beam was divided using a beam splitter. Half of the output was focused using a lens on a VIS-SWIR camera (Ninox-640) to monitor the output facet and guarantee precise alignment of both input and output beams. The second half of the output beam was coupled into a single-mode fiber using an Olympus objective 0.25 NA with x10 magnification. The output data collection setup, mounted on a 3-axis stage, included a fiber connected to an optical spectrum analyzer (Yokogawa 6370D) with a resolution of 2 nm. This comprehensive configuration facilitated the precise analysis and control of the optical signals in the rib waveguide system.

3. Results

3.1. Rib waveguides composition

First, we studied the conventional spectrum of the N-methylaniline in a hexane mixture and selected the optimal concentration for further studies of the mixtures on modified waveguides. We performed a detailed study to find the optimal concentration using a Fourier-transform infrared spectroscopy (FTIR). The data is presented in Fig. 2.

We found that the N–H stretching vibrations are well-presented in the range of 3300–3500 cm^{-1}. Typically, the asymmetric stretching mode is around 3500 cm^{-1}, while the symmetric mode appears around 3400 cm^{-1}. These vibrational frequencies are known to exhibit small variations with changes in solvent polarity. Additionally, more substantial changes in these vibrational frequencies can be observed in concentrated solutions where intermolecular association occurs. Understanding these spectral features is crucial for interpreting infrared spectra and gaining insights into molecular interactions, especially in solutions with varying concentrations and solvent environments. In our case, the peaks are at 3490 cm^{-1}. The C–H symmetric and asymmetric stretching frequencies, particularly in the methyl group, have been extensively studied for a series of substituted anilines. In the case of N-methyl and dimethyl anilines, assign the infrared bands at 2812 and 2801 cm^{-1} as C–H symmetric stretching vibrations. Additionally, they identify the bands at 2855.65 and 2879.45 cm^{-1} as C–H asymmetric stretching vibrations for N-methyl and dimethyl anilines, respectively. These vibrational frequencies provide valuable information about the molecular structure and bonding environment of the methyl groups in these compounds [48,49]. From the graphs, we see how the peaks of N-methylaniline change when the hexane concentration changes; already at a ratio of 1 to 5, the peaks become barely distinguishable. Therefore, we decided to use modified rib waveguides with a concentration of 1:3 for our experiments. Peaks are not shifted depending on concentrations.

Table 1
Elemental composition of the glass substrate with palladium nanorods with a concentration of 100 μg/ml.

Element	Atomic conc. (%)	Weight conc. (%)
C	38.392	26.226
O	36.517	33.233
Na	5.815	7.608
Mg	1.085	1.502
Al	1.762	2.703
Si	14.347	22.923
Ca	1.800	4.104
Pd	0.281	1.762

In addition, we studied the composition of gold nanorods palladium coated on the surface of a glass substrate using energy-dispersive X-ray spectroscopy (EDS). First, we dripped nanorods in water with a concentration of 100 μg/ml on a glass slide and dried it. Fig. 3a shows a Scanning electron microscopy (SEM) image of the sample and highlights the EDS study area with a size of $S1 = 489.05$ mm^2. The bright particles are related to gold nanorods with a palladium layer, which covers individual areas of the substrate and forms clusters of conglomerates. The large dark particles are related to Al_2O_3 nanoparticles. We found that using nanorods with a concentration of 100 μg/ml, the obtained surface modification is a complex surface layer with randomly varying-sized particles. Therefore, we decided to use a lower concentration of nanorods in water to achieve a uniform layer of known size. We dripped nanorods in water with a concentration of 10 μg/ml on a new glass slide and dried it. Fig. 3b shows an SEM image of a sample with a concentration of nanorods of 10 μg/ml in water with highlighted EDS area size of $S2 = 11.25$ mm^2. The image shows that the gold nanorods with palladium form a uniform single layer area.

The EDS data of glass substrate with nanorods with a concentration of 100 μg/ml in water (Fig. 3a) in Table 1 shows that the samples consist of carbon, oxygen, sodium, magnesium, silicon, aluminum and calcium, substances which are related to the glass composition. The palladium atomic concentration of the total composition is 0.281%. The aluminum atomic concentration of the total composition is 1.762%. Gold was not detected since its percentage in the total mass of the sample was too small.

The EDS spectra of the glass substrate with nanorods with a concentration of 10 μg/ml in water (Fig. 3b) in Table 2 show higher concentrations of palladium and gold. Palladium concentrations were 5.886%, gold 0.503%, and aluminum 1.166%. The remaining substances are from the glass substrate.

Based on the data obtained by the EDS method and the calculation, we concluded that the concentration of nanorods in the water of

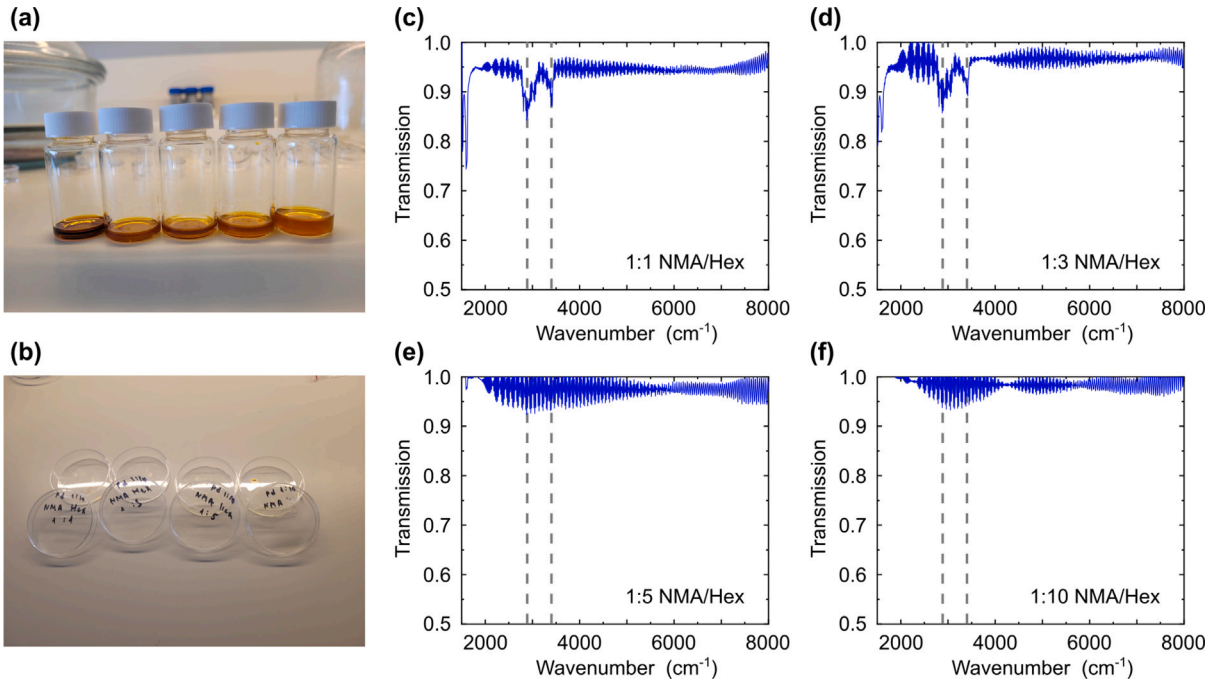

Fig. 2. Fourier-transform infrared (FTIR) spectroscopy results. (a) Samples with different concentrations of N-methylaniline in hexane and (b) glass slides with palladium layer (concentration of 10 μg/ml in water) with the samples deposited on them. FTIR spectra of glass samples with a concentration of (c) 1:1 N-methylaniline to hexane, (d) 1:3 N-methylaniline to hexane, (e) 1:5 N-methylaniline hexane and (f) 1:10 N-methylaniline hexane.

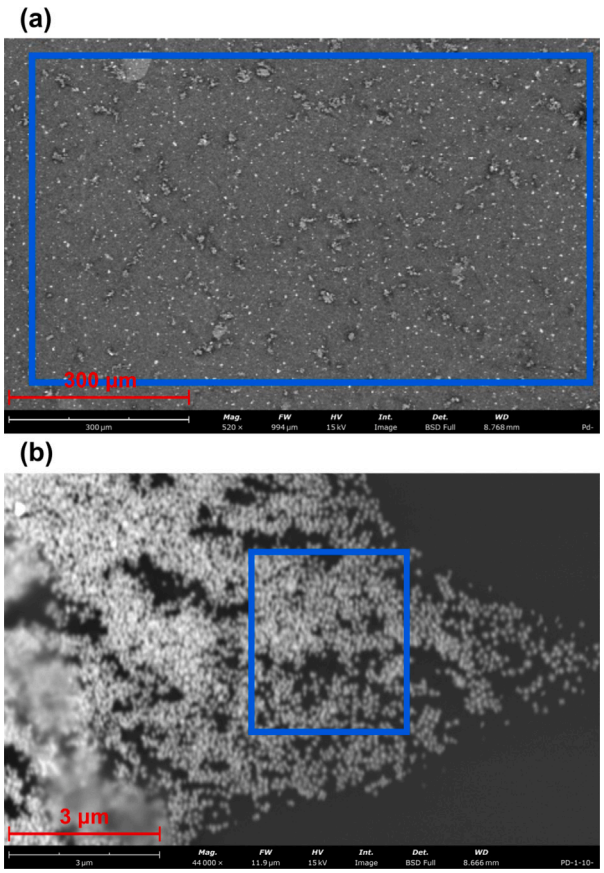

Fig. 3. Scanning electron microscopy with EDS image of glass substrate with gold nanorods palladium coated with (a) concentration of 100 μg/ml in water and (b) concentration of 10 μg/ml in water. The EDS area is marked with a blue square.

Table 2
Elemental composition of the glass substrate with palladium nanorods with a concentration of 10 μg/ml.

Element	Atomic conc. (%)	Weight conc. (%)
C	27.181	13.500
N	3.625	2.100
O	36.271	24.000
Na	5.782	5.500
Mg	1.094	1.100
Al	1.166	1.300
Si	16.442	19.100
Ca	2.051	3.400
Pd	5.886	25.900
Au	0.503	4.100

Table 3
Elemental composition of the top surface of a rib waveguide.

Element	Weight concentration (%)
Ta	80.4
O	19.6

10 μg/ml is optimal for the layer on the surface of the waveguide to be a single layer of nanorods and nanoparticles. Next, we studied the composition of a rib waveguide before and after the deposition of palladium nanorods on top of the waveguide. The elemental composition of rib waveguide clean rib waveguide and rib waveguide with palladium nanorods is shown in Tables 3 and 4, respectively.

Table 3 shows the elemental composition of a clean rib waveguide. It shows the presence in the composition of a Ta_2O_5 film on the surface of the rib waveguide, which is used to cover the waveguide to protect and prevent oxidation of its surface and change the refractive index. This material also minimizes losses and provides precise control over the light path, improving waveguide performance.

Table 4 shows the rib waveguide surface elemental composition after modifying its surface with palladium nanorods. The tantalum

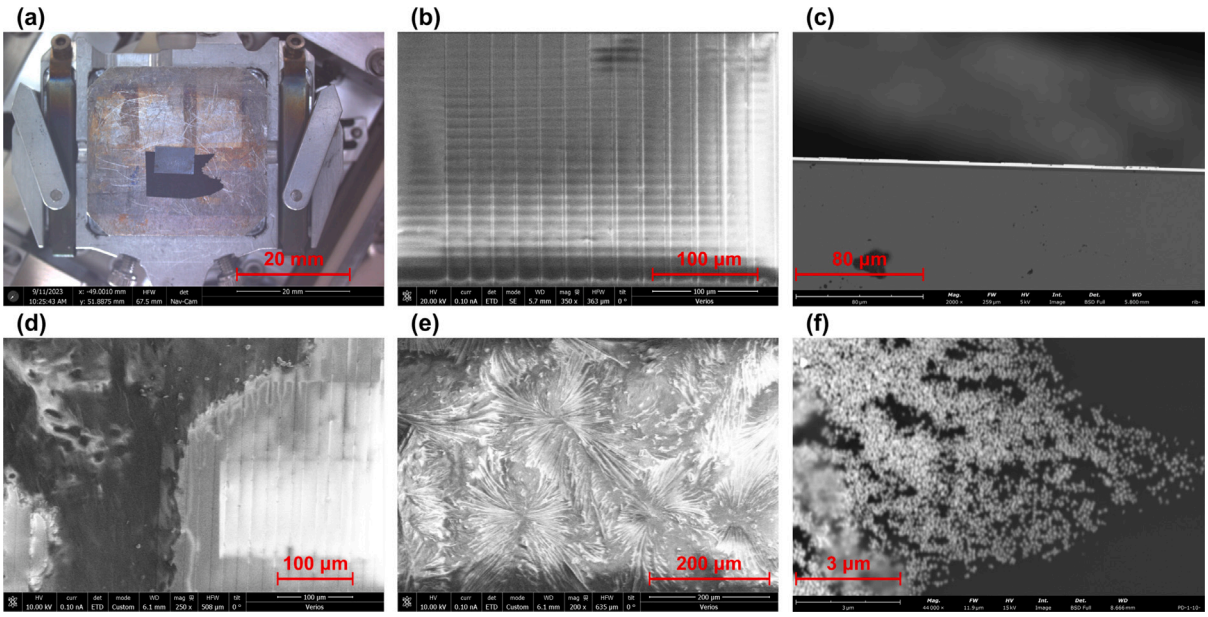

Fig. 4. Scanning electron microscope (SEM) images. (a) a photograph of a rib waveguide with palladium positioned on the scanning electron microscope holder. (b) Top view and (c) side view of the surface of a clean rib waveguide. (d) Rib waveguide with palladium nanorods deposited on the top of the waveguide while the palladium nanorods in water had a 100 µg/ml concentration. (e) Zoomed-in image of rib waveguide with palladium. (f) Rib waveguide with palladium nanorods deposited on the top of the waveguide while the palladium nanorods in water had a concentration of 10 µg/ml.

Table 4
Elemental composition of the top surface of a rib waveguide with Pd nanorods.

Element	Weight concentration (%)
Ta	76.4
O	14.7
Al	4.6
Pd	4.3

concentration changes by 4%, oxygen concentration changes by 4.9%, and palladium and aluminum appear, which indicates the physical adsorption of particles, as well as palladium and aluminum appear, which indicates the physical adsorption of particles, as well as chemical reaction of oxygen replacement. Tantalum reacted more with aluminum nanoparticles than with palladium. The presence of aluminum in the sample is due to the presence of an impurity in the palladium samples; aluminum was used at one of the stages of producing nanorods. In our work, aluminum is an admixture necessary to increase the absorption of hydrogen-containing substances. We do not see the presence of gold since there are many other substances.

Fig. 4 shows the rib waveguide before and after the deposition of gold nanorods palladium coated, a study conducted using a scanning electron microscope (SEM). Fig. 4a shows a modified waveguide located in a SEM setup. Fig. 4b shows the clean surface of the waveguide, on which one group of waveguides are visible, showing strips with varying widths where the wider strip is 20 µm wide and the smaller is 9.9 µm wide. Fig. 4c shows a side view of the waveguide showing rib waveguide with a strip height of 400 nm. It is also visible on the side that a uniform layer of Ta_2O_5 is applied to the surface of the rib waveguide. Figs. 4d and 4e show a waveguide with a palladium layer (concentration of 100 µg/ml) and a clean area. The particles form a dense layer on the waveguide surface, rendering the waveguide nearly invisible. The concentration was diluted to 1 part nanorods to 10 parts distilled water to address this. In Fig. 4g, a waveguide with a palladium layer (nanorods concentration in water of 10 µg/ml) is shown, where nanorods cluster without adhering to each other, forming a homogeneous layer on several edges of the rib waveguide.

3.2. Experimental results

To assess the performance of the modified rib waveguide in a molecular environment, we designed an experimental setup as shown in Fig. 5a. A broadband laser source was coupled to a single-mode fiber using an objective. The single-mode fiber was connected to an optical spectrum analyzer to achieve maximal coupling efficiency. Next, the optical fiber was connected to a reflective collimator to create a collimated beam which was focused by a long working distance objective on the input facet of the waveguide (Fig. 5b). The rib waveguide was positioned on a 3-axis linear stage with a 2-axis rotation stage and was monitored using an x100 magnification microscope for accurate alignment. The output of the waveguide was collected with a long working distance objective. The output beam was split into two parts by a beam splitter. Half of the beam was directed to a camera, facilitating facet and mode imaging studies, and half was measured using a spectrum analyzer. Both the camera and the spectrum analyzer were used in parallel to optimize the input and output coupling. The transmission spectrum was measured at a wavelength range of 1300–1600 nm. The wavelengths range was chosen to overlap with the absorption of the first overtone of the N–H bond of N-methylaniline (NMA) that appears at 1.496 µm [21,50]. The experimental results are shown in Figs. 5c–f.

Figs. 5c–d show the coupled light in at the input facet and the output facet, respectively. The transmittance of pure and nanorod-coated rib waveguides in air was measured to obtain a reference spectrum. Next, a 5 µl solution of N-methylaniline with hexane was dropped on the modified rib waveguides with palladium nanorods, and the transmission was measured. Fig. 5e shows the transmission of a pure rib waveguide (blue graph) and a modified rib waveguide with N-methylaniline with hexane (red curve) at a wavelength range of 1300–1600 nm. Absorption bands appear at wavelengths of 1379 nm, 1448 nm, and 1589 nm. The first two peaks are attributed to C–H bones and the last to N–H bonds. Fig. 5f shows normalized transmission of hexane in water (concentration 1 to 1) on a modified rib waveguide. In this representation, the characteristic peaks of hexane are more clearly distinguishable. This visualization aids in identifying and analyzing the distinct features associated with each substance, providing valuable insights into their presence and interactions on the palladium surface.

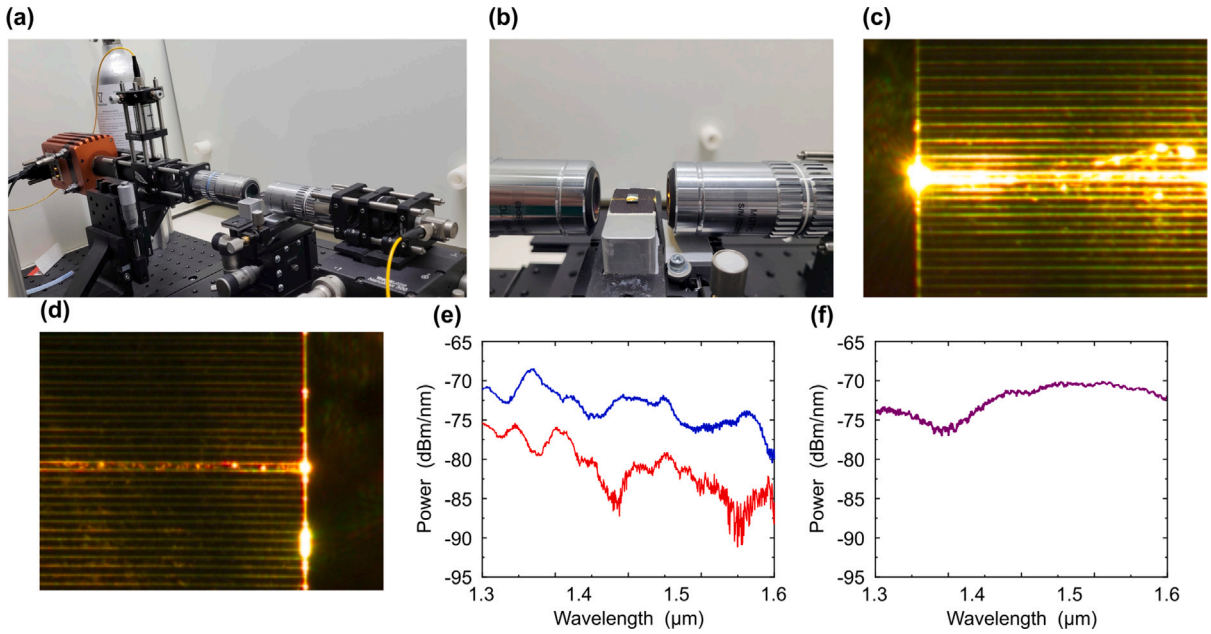

Fig. 5. (a) The experimental setup and (b) zoom in on the modified rib waveguide with palladium nanorods. Microscope top view images of (c) the input and (d) output facets. (e) Measured transmission spectra at a wavelengths range of 1.3-1.6 μm modified rib waveguides with palladium nanorods with a mixture of N-methylaniline in hexane (red curve) with a concentration of 1:3 (NMA/hexane) and clean rib waveguide (blue curve). (f) Normalized transmission spectra at a wavelength range of 1.3-1.6 μm of modified rib waveguide with hexane in water 1:1.

In hexane in water, the absorption appears at a wavelength of 1379 nm (CH_3) with a drop of 5.5 dB and a blue-shifted peak. There is a peak at 1448 nm (CH_2) with a drop of 1.5 dB. Both peaks are attributed to the C–H bonds of hexane. For the first time, we obtained peaks of an easily evaporated substance in a small volume of 5 μl, attributing this observation to the presence of palladium.

3.3. Numerical simulation

To explore how light interacts with gold and palladium nanorods on a rib waveguide, we built a numerical simulation model using Lumerical FDTD. A silicon-on-insulator waveguide with a height of 2 μm, strip width of 16 μm and strip height of 400 nm as illustrated in Fig. 6a. The simulation was performed at a wavelength of 1.5 μm, corresponding to the absorption of the first overtone of the N–H bond in N-methylaniline. The simulation was performed for a clean waveguide and a waveguide with palladium nanorod to observe the nanorod's influence on the evanescent field that interacts with the analyte. The palladium nanorod was placed on the top of the waveguide strip in two configurations: perpendicular (Fig. 6d) and parallel (Fig. 6g) to the mode propagation direction. Around the nanorods, a much smaller mesh was defined for obtaining an accurate electric field around the nanorods. The numerical results are shown in Fig. 6.

The electric field in the center of nanorods is shown at Figs. 6(b, e, h) for $y = 0$ μm (xz plane) and Figs. 6(c, f, i) for $x = 5$ μm (yz plane). The field is enhanced parallel to the light propagation direction while placing palladium nanorod. Next, we calculated the absorption of the rib waveguide with a mixture of N-methylaniline in hexane with a concentration of 1:3 (NMA/hexane) as an analyte for fundamental TE and TM modes. The numerical results are shown in Fig. 7. We found that the absorption for TE and TM modes for hexane are around 0.05 and 0.15 dB/cm, respectively. In our experiment for rib waveguide with palladium nanorods, the absorption peak of hexane was around 4 dB for a waveguide length of 5 mm which is an enhancement of 100. The enhancement is caused by the palladium nanorods, which are bound to the hexane, increasing the absorption.

4. Conclusion

Optical waveguides can find widespread applications across various industries, particularly in detecting and monitoring substances in the environment. They are crucial in environmental protection initiatives, contributing to water, soil, and air pollution control. In air pollution, rib waveguides are especially valuable due to palladium's high sorption capacity for hydrogen, a common component in gas mixtures. This technology can be instrumental in determining the concentration of hydrogen mixtures, particularly in energy production.

Our research encompassed the fabrication and thorough testing of modified rib waveguides to detect substances and their concentrations in air and water. We performed a combination of numerical modeling and experimental studies, providing a comprehensive approach to understanding and assessing the performance of these waveguides in diverse environmental conditions. The results showed that by modifying the rib waveguide with palladium nanorods, the transmission of the entire waveguide improves, and the sensitivity of the waveguide increases. In addition, the palladium nanorods bond with the hydrogen atoms in hexane, preventing the evaporation of the hexane and increasing the absorption. In our experiment, we found an increase in the absorption of both N-methylaniline and hexane, while in the case of hexane, the absorption was more significant and distinguishable. According to our numerical studies, the peaks of hexane should be much smaller, but provided that palladium has the property of attracting hydrogen, the absorption increases 100 times as compared to the numerical results.

Therefore, we conclude that the utility of modified rib waveguides extends to hazardous industries and disaster zones, where they enable the accurate detection of low concentrations of substances. This capability is valuable in enhancing safety measures and response strategies in critical situations. The versatility Pd coated nanoparticles on rib waveguides positions them as valuable tools with various applications, contributing significantly to environmental monitoring and safety protocols.

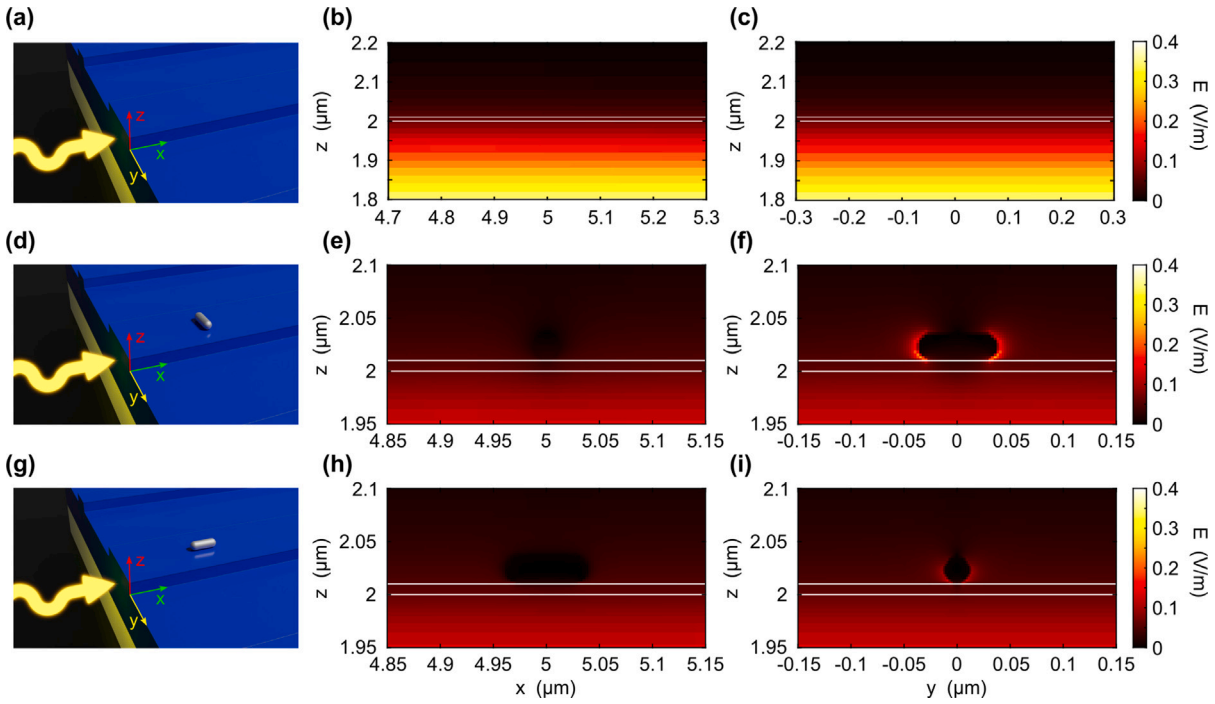

Fig. 6. Numerical simulation of a rib waveguide for three configurations: (a) clean waveguide, with (d) palladium nanorod perpendicular to propagation direction and (g) nanorod parallel to propagation direction. The electric field at a wavelength of 1.5 μm was calculated in the center of the nanorod at (b, e, h) $y = 0$ μm (xz plane) and (c, f, i) $x = 5$ μm (yz plane).

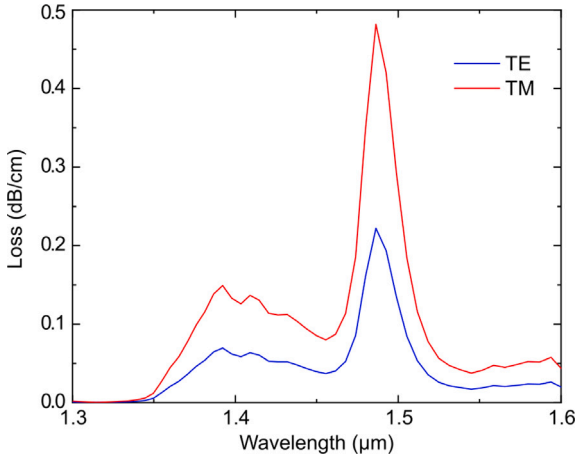

Fig. 7. Numerical simulation for the losses of a rib waveguide with a mixture of N-methylaniline in hexane with a concentration of 1:3 (NMA/hexane) for fundamental TE and fundamental TM modes.

CRediT authorship contribution statement

Anastasia Novikova: Methodology, Investigation, Validation, Writing – original draft. **Aviad Katiyi:** Investigation, Methodology, Validation, Visualization, Writing – original draft. **Alina Karabchevsky:** Writing – review & editing, Resources, Project administration, Investigation, Funding acquisition, Conceptualization.

Declaration of competing interest

The authors declare the following financial interests/personal relationships which may be considered as potential competing interests: Alina Karabchevsky reports financial support was provided by Ben-Gurion University of the Negev. If there are other authors, they declare that they have no known competing financial interests or personal relationships that could have appeared to influence the work reported in this paper.

Data availability

Data will be made available on request.

Acknowledgments

This research was supported by the Ministry of Science & Technology, Israel- Grant #0006276. The authors acknowledge Mr Uzziel Sheintop for constructing the experimental set-up.

References

[1] A. Karabchevsky, A. Katiyi, A.S. Ang, A. Hazan, On-chip nanophotonics and future challenges, Nanophotonics 9 (12) (2020) 3733–3753.
[2] Z. Wang, H. Chen, Y.-P. Teng, Role of greener energies, high tech-industries and financial expansion for ecological footprints: Implications from sustainable development perspective, Renew. Energy 202 (2023) 1424–1435.
[3] O.G. Aralovna, O.B. Nurillaevich, A.S. Ayonovna, Y.K. Manzarov, Ecological globalization and its social place in the globalization system of processes, J. Surv. Fish. Sci. 10 (1S) (2023) 5000–5006.
[4] A. Novikova, A. Karabchevsky, Green extraction of graphene from natural Mineral Shungite, Nanomaterials 12 (24) (2022) 4356.
[5] A. Novikova, A. Katiyi, A. Halstuch, A. Karabchevsky, Green-graphene protective overlayer on optical microfibers: Prolongs the device lifetime, Nanomaterials 12 (17) (2022) 2915.
[6] A. Karabchevsky, A. Katiyi, M.I.M. Bin Abdul Khudus, A.V. Kavokin, Tuning the near-infrared absorption of aromatic amines on tapered fibers sculptured with gold nanoparticles, ACS Photonics 5 (6) (2018) 2200–2207.
[7] X. Liu, R. Singh, G. Li, C. Marques, B. Zhang, S. Kumar, WaveFlex biosensor-using novel tri-tapered in tapered four-core fiber with multimode fiber coupling for detection of aflatoxin B1, J. Lightwave Technol. (2023).
[8] G. Lopes, N. Cennamo, L. Zeni, R. Singh, S. Kumar, A.J. Fernandes, F. Costa, S.O. Pereira, C. Marques, Innovative optical pH sensors for the aquaculture sector: Comprehensive characterization of a cost-effective solution, Opt. Laser Technol. 171 (2024) 110355.

[9] R. Singh, Z. Wang, C. Marques, R. Min, B. Zhang, S. Kumar, Alanine aminotransferase detection using TIT assisted four tapered fiber structure-based LSPR sensor: From healthcare to marine life, Biosens. Bioelectron. 236 (2023) 115424.

[10] W. Zhang, R. Singh, Z. Wang, G. Li, Y. Xie, R. Jha, C. Marques, B. Zhang, S. Kumar, Humanoid shaped optical fiber plasmon biosensor functionalized with graphene oxide/multi-walled carbon nanotubes for histamine detection, Opt. Express 31 (7) (2023) 11788–11803.

[11] A. Karabchevsky, U. Sheintop, A. Katiyi, Overtone spectroscopy for sensing—Recent advances and perspectives, ACS Sens. 7 (10) (2022) 2797–2803.

[12] A. Katiyi, A. Karabchevsky, Deflected talbot-mediated overtone spectroscopy in near-infrared as a label-free sensor on a chip, ACS Sens. 5 (6) (2020) 1683–1688.

[13] D. Yuan, Y. Dong, Y. Liu, T. Li, Design of a high-performance micro integrated surface plasmon resonance sensor based on silicon-on-insulator rib waveguide array, Sensors 15 (7) (2015) 17313–17328.

[14] M. Butt, S. Khonina, N. Kazanskiy, Modelling of rib channel waveguides based on silicon-on-sapphire at 4.67 μm wavelength for evanescent field gas absorption sensor, Optik 168 (2018) 692–697.

[15] C.D. Lyons, S. Katz, R. Bartha, Mechanisms and pathways of aniline elimination from aquatic environments, Appl. Environ. Microbiol. 48 (3) (1984) 491–496.

[16] N. Yoshimi, S. Sugie, H. Iwata, K. Niwa, H. Mori, C. Hashida, H. Shimizu, The genotoxicity of a variety of aniline derivatives in a DNA repair test with primary cultured rat hepatocytes, Mutat. Res./Genet. Toxicol. 206 (2) (1988) 183–191.

[17] M.V. Kulkarni, A.K. Viswanath, P. Khanna, Synthesis and characterization of poly (N-methyl aniline) doped with sulphonic acids: Their application as humidity sensors, J. Appl. Polym. Sci. 99 (3) (2006) 812–820.

[18] S.R. Clough, Hexane, in: P. Wexler (Ed.), Encyclopedia of Toxicology, 3rd ed., 2014, pp. 900–904.

[19] D.G. Graham, V. Amarnath, W.M. Valentine, S.J. Pyle, D.C. Anthony, Pathogenetic studies of hexane and carbon disulfide neurotoxicity, Crit. Rev. Toxicol. 25 (2) (1995) 91–112.

[20] D. Couri, M. Milks, Toxicity and metabolism of the neurotoxic hexacarbons n-hexane, 2-hexanone, and 2, 5-hexanedione, Annu. Rev. Pharmacol. Toxicol. 22 (1) (1982) 145–166.

[21] A. Katiyi, A. Karabchevsky, Figure of merit of all-dielectric waveguide structures for absorption overtone spectroscopy, J. Lightwave Technol. 35 (14) (2017) 2902–2908.

[22] A. Katiyi, A. Karabchevsky, Si nanostrip optical waveguide for on-chip broadband molecular overtone spectroscopy in near-infrared, ACS Sens. 3 (3) (2018) 618–623.

[23] A. Rickman, G. Reed, F. Namavar, Silicon-on-insulator optical rib waveguide loss and mode characteristics, J. Lightwave Technol. 12 (10) (1994) 1771–1776.

[24] W. Huang, H.A. Haus, A simple variational approach to optical rib waveguides, J. Lightw. Technol. 9 (1) (1991) 56–61.

[25] H. Benisty, M. Besbes, Confinement and optical properties of the plasmonic inverse-rib waveguide, J. Opt. Soc. Amer. B 29 (4) (2012) 818–826.

[26] S. Jainth, S. Dahiya, S. Kumar, Design and simulation of strip loaded and rib waveguide with integration of 2D material, Indian J. Sci. Technol. 13 (40) (2020) 4262–4274.

[27] L. Vivien, S. Laval, B. Dumont, S. Lardenois, A. Koster, E. Cassan, Polarization-independent single-mode rib waveguides on silicon-on-insulator for telecommunication wavelengths, Opt. Commun. 210 (1–2) (2002) 43–49.

[28] E. Cassan, S. Laval, S. Lardenois, A. Koster, On-chip optical interconnects with compact and low-loss light distribution in silicon-on-insulator rib waveguides, IEEE J. Sel. Top. Quantum Electron. 9 (2) (2003) 460–464.

[29] D. Yevick, B. Hermansson, New formulations of the matrix beam propagation method: Application to rib waveguides, IEEE J. Quantum Electron. 25 (2) (1989) 221–229.

[30] M. Shahbaz, Ł. Kozłowski, M.A. Butt, R. Piramidowicz, Mitigating the bending losses of the silica-titania-based rib waveguide structure, Opto-Electron. Rev. 31 (2023) e145551.

[31] B. Robert, R. Pélissier, R. Escalier, A. Mehdi, C. Gergely, C. Vigreux, Strategies for selective functionalization of amorphous chalcogenide rib waveguides, Opt. Mater. 127 (2022) 112327.

[32] H.R. Sultan, M.F. Jaddoa, F.F.K. Husain, Modeling of asymmetric rib SOI waveguide for optical communications applications, in: AIP Conference Proceedings, Vol. 2398, No. 1, AIP Publishing, 2022.

[33] W. Zhang, R. Singh, F.-Z. Liu, C. Marques, B. Zhang, S. Kumar, WaveFlex biosensor: a flexible-shaped plasmonic optical fiber sensor for histamine detection, IEEE Sens. J. (2023).

[34] D.M. da Silva, L.R.P. Kassab, A.L. Siarkowski, C.B. de Araújo, Influence of gold nanoparticles on the 1.53 μm optical gain in Er 3+/Yb 3+: PbO-GeO 2 RIB waveguides, Opt. Express 22 (13) (2014) 16424–16430.

[35] H. Benisty, M. Besbes, Plasmonic inverse rib waveguiding for tight confinement and smooth interface definition, J. Appl. Phys. 108 (6) (2010).

[36] N. Carriere, M. Alam, M. Mojahedi, J.S. Aitchison, An integrated optical hydrogen sensor on a silicon-on-insulator platform: Effects of palladium film thickness, Sensors Actuators B 216 (2015) 6–10.

[37] P. Karasiński, C. Tyszkiewicz, R. Rogoziński, Rib waveguides based on the sol-gel derived SiO2: TiO2 films, Photonics Lett. Poland 2 (1) (2010) 40–42.

[38] J. Wang, L. Zhang, Y. Chen, Y. Geng, X. Hong, X. Li, Z. Cheng, Saturable absorption in graphene-on-waveguide devices, Appl. Phys. Express 12 (3) (2019) 032003.

[39] T. Ma, S. Liu, Y. Tian, H. Liu, F. Wang, Refractive index sensing based on graphene-hBN-silicon hybrid plasmonic rib waveguide, IEEE Sens. J. 21 (15) (2021) 16598–16605.

[40] A. Hazan, B. Ratzker, D. Zhang, A. Katiyi, M. Sokol, Y. Gogotsi, A. Karabchevsky, Mxene-nanoflakes-enabled all-optical nonlinear activation function for on-chip photonic deep neural networks, Adv. Mater. 35 (11) (2023) 2210216.

[41] O. Lyutakov, J. Tuma, V. Prajzler, I. Huttel, V. Hnatowicz, V. Švorčík, Preparation of rib channel waveguides on polymer in electric field, Thin Solid Films 519 (4) (2010) 1452–1457.

[42] V. Prajzler, J. Klapuch, O. Lyutakov, I. Hüttel, J. Špirková, P. Nekvindová, V. Jeřábek, Design, Fabrication and Properties of Rib Poly (Methylmethacrylimide) Optical Waveguides, Radioengineering Society, 2011.

[43] M.W. Austin, GaAs/GaAlAs curved rib waveguides, IEEE Trans. Microw. Theory Tech. 30 (4) (1982) 641–646.

[44] T. Lewi, A. Katzir, Silver halide integrated waveguides for sensing applications in the mid-infrared, in: Infrared Sensors, Devices, and Applications II, vol. 8512, SPIE, 2012, pp. 69–76.

[45] C. Vigreux, E. Barthélémy, L. Bastard, J.-E. Broquin, M. Barillot, S. Ménard, G. Parent, A. Pradel, Realization of single-mode telluride rib waveguides for mid-ir applications between 10 and 20 μm, Opt. Lett. 36 (15) (2011) 2922–2924.

[46] F. Lewis, The palladium-hydrogen system, Platinum Met. Rev. 26 (1) (1982) 20–27.

[47] N. Comisso, S. Daolio, G. Mengoli, R. Salmaso, S. Zecchin, G. Zotti, Chemical and electrochemical synthesis and characterization of polydiphenylamine and poly-n-methylaniline, J. Electroanal. Chem. Interfacial Electrochem. 255 (1–2) (1988) 97–110.

[48] P. Yella Reddy, T.S. Krishna, M. Gowrisankar, K. Siva Kumar, C.N.S.S. Pavan Kumar, FTIR Spectra of pure components and their binary liquid components (Binary mixtures of formamide with aniline, N-methyl aniline and N, N-dimethyl aniline), Int. J. Ambient Energy 43 (1) (2022) 5327–5343.

[49] R.G. Arokiaraj, R. Raju, S. Ravikumar, K. Sivakumar, P. Bhanuprakash, V. Pandiyan, Excess thermodynamic properties and FTIR studies of binary mixtures of aniline with esters at different temperatures, Chem. Data Collect. 37 (2022) 100807.

[50] A. Karabchevsky, A. Kavokin, Giant absorption of light by molecular vibrations on a chip, Sci. Rep. 6 (1) (2016) 21201.